Pressure-Induced Two-Color Photoluminescence in MnF_2 at Room Temperature

I. Hernández,[1] Fernando Rodríguez,[1,*] and H. D. Hochheimer[2]

[1]*DCITIMAC, Facultad de Ciencias, University of Cantabria, 39005 Santander, Spain*

[2]*Department of Physics, Colorado State University, Fort Collins, Colorado 80523, USA*

(Received 17 January 2007; published 12 July 2007)

A novel two-color photoluminescence (PL) is found in MnF_2 at room temperature under high pressure. Contrary to low-temperature PL, PL at room temperature is unusual in transition-metal concentrated materials like MnF_2, since the deexcitation process at room temperature is fully governed by energy transfer to nonradiative centers. We show that room-temperature PL in MnF_2 originates from two distinct Mn^{2+} emissions in the high-pressure cotunnite phase. The electronic structure and the excited-state dynamics are investigated by time-resolved emission and excitation spectroscopy at high pressure.

DOI: 10.1103/PhysRevLett.99.027403 PACS numbers: 78.55.−m, 71.35.−y, 71.70.Gm, 81.40.Vw

Transition-metal ions are often used as efficient photoluminescence (PL) centers in compounds like (Ca, Mg)F_2: Mn^{2+} [1–3], Al_2MgO_4: Co^{2+} [4], $KMgF_3$: Ni^{2+} [5,6], MgF_2: Co^{2+} [3,7], Al_2O_3: Cr^{3+} [8,9], Al_2O_3: Ti^{3+} [10,11], or $YAlO_3$: Mn^{3+} [12,13]. Hence, transition-metal-doped materials have received considerable attention for their capability as scintillators, optical sensors and memories, laser media, etc. [14,15]. Despite the intense research aimed to improve PL in materials, the microscopic processes governing excited-state deexcitation yielding PL are still not understood fully. Therefore, prediction of whether a given transition-metal-related material shows PL at ambient conditions or under pressure and temperature is in many cases uncertain. A puzzling behavior concerns the loss of PL with increasing transition-metal concentration, which is quenched in most concentrated materials at room temperature (RT). Transition-metal fluorides and oxides such as MnF_2, CoF_2, NiF_2, Cr_2O_3, Ti_2O_3, Mn_2O_3 illustrate this behavior [8,15,16]. The unlikely nonradiative deexcitation observed in concentrated materials is explained in terms of exciton migration and subsequent transfer to nonradiative traps (exciton capture centers), which are eventually responsible for the absence of RT PL [8,16] (Fig. 1). Today, the knowledge of the excited-state dynamics in exchange coupled systems still remains a challenge [17]. The activation energies associated with exciton migration and transfer to nonradiative traps depend on the crystal structure, and thus can be modified through structural modifications induced by changes of chemical composition or phase transformation prompted by temperature or pressure [18]. Usual strategies aimed at finding out new methods for the control of exciton migration and trapping are mainly focused on the passivation of nonradiative traps through purification and doping with efficient PL centers [19,20]. Nevertheless, structural changes yielding modifications of the transition-metal local structure and exchange pathway yet remain unexplored.

MnF_2 [16] has been a model material for investigating exciton migration and trapping through selective doping with alkaline-earth-metal and rare-earth-metal atom traps acting as centers for exciton capture and selective emission [20–22]. As a result, the excited-state dynamics related to Mn^{2+} $^4T_1$ excitons and their capture by PL and nonradiative traps is well understood in terms of the MnF_2 rutile structure following the scheme of Fig. 1. The temperature dependence of the red emission band indicates that PL is quenched for $T > 120$ K in the purest MnF_2 single crystal [23] and $T > 200$ K for MnF_2 nanocrystals [24].

Here we report a novel procedure to obtain PL in MnF_2 at RT by applying high pressure. The idea consists of inducing structural transformations in MnF_2, as long as (i) they provide more efficient PL sites for Mn^{2+} [1,2], and (ii) they reduce exciton migration and transfer through changes in the Mn-F-Mn exchange pathway [8]. MnF_2 exhibits at RT an interesting phase transition sequence: it transforms with increasing pressure from rutile (TiO_2) to fluorite (CaF_2), cotunnite (α-$PbCl_2$) and scrutyinite (α-PbO_2), each providing different Mn^{2+} coordination and Mn-F-Mn paths [25]. The high-pressure phases fulfill structural requirements to reduce the nonradiative probability by multiphonon relaxation within Mn^{2+}, and also to inhibit exciton migration within the lattice. Spectroscopy at high pressure has revealed that radiative and nonradiative processes governing PL in Mn^{2+}-doped fluorite crystals ($Ca_{1-x}Sr_xF_2$) mainly depend on the host site volume [1]. As a result, we have induced PL at RT in the nonphotoluminescent Mn^{2+}-doped SrF_2 and BaF_2 by applying high pressure [2].

The PL properties of MnF_2 at high pressure are investigated to elucidate whether high-pressure phases enable PL at RT, and to identify the PL centers and their excited-state dynamics by means of time-resolved emission and excitation spectroscopy under pressure. The high-purity float-zone grown MnF_2 single crystals and spectroscopic setups employed here are described elsewhere [2,23,24,26].

The low-temperature MnF_2 PL at 2.12 eV (585 nm) corresponds to the $^4T_1 \rightarrow {}^6A_1$ transition (Fig. 1) within the nearly O_h-symmetry $(MnF_6)^{4-}$ unit of the rutile structure. As Fig. 2 shows, the red emission is unlike the green emission observed in both eightfold (O_h) and fourfold (T_d) coordinations in Mn^{2+} halides, which is explained by their

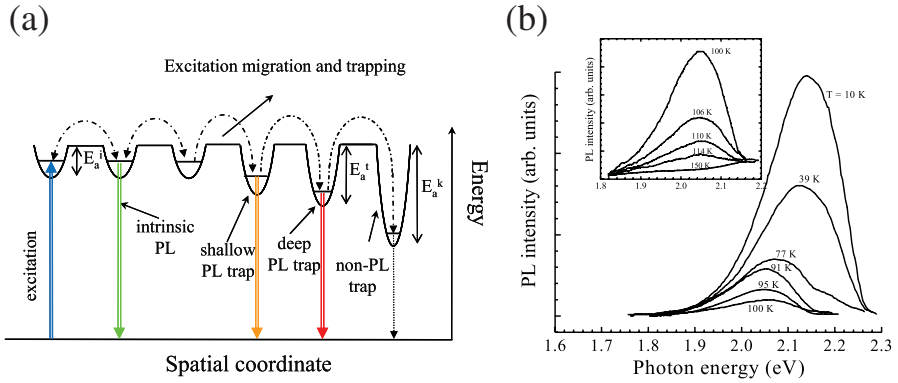

FIG. 1 (color). (a) Schematic representation of migration and trapping of $^4T_1$ excitons in MnF_2 yielding intrinsic photoluminescence (PL), Mn^{2+}-perturbed PL, and nonradiative processes. E_a is the activation energy for thermal detrapping. (b) The variation of the emission spectrum of MnF_2 with temperature illustrates the PL trapping and quenching involved in the deexcitation processes. Note that the PL redshifts with increasing temperature and is quenched above 114 K in a float-zone grown MnF_2 single crystal.

weaker crystal field as compared to sixfold coordination (O_h) [1,27]. The absorption (or excitation) spectrum associated with Mn^{2+} reflects its local symmetry and crystal field in fluorides with different coordination numbers (Fig. 2) [27].

At ambient pressure, the MnF_2 emission shifts towards lower energies with increasing temperature due to population of deeper Mn^{2+} centers, and is quenched for $T >$ 120 K (Fig. 1). Although the nature of nonradiative centers remains unknown yet, Mn^{3+} traces (<1 ppm) can partially account for the PL quenching at RT in MnF_2 [23,28]. The variation of the MnF_2 emission spectrum with pressure, which is shown in Fig. 3, indicates that PL remains quenched at RT up to 13 GPa. However, a new pressure-induced two-color PL appears at RT for pressures above 14 GPa in the cotunnite phase. The PL spectrum consists of two emission bands at 2.34 and 1.87 eV, which we associate with two different Mn^{2+} centers: a regular Mn^{2+} site (S) and a strongly perturbed Mn^{2+} site (D), respectively. The assignment is based on the variation of PL and its associated excitation spectra with pressure for different Mn^{2+} coordination (Fig. 2). Both emissions correspond to the same excitation spectrum, and thus indicate that red PL mainly occurs through energy transfer from nearby ninefold-coordinated Mn^{2+} in the high-pressure cotunnite phase. Actually, their excitation spectrum at 16.5 GPa consists of an unresolved band around 2.8 eV (450 nm), and a sharp excitation near 3.0 eV (410 nm). Except for wavelength limitations imposed by the excitation source, the spectrum resembles the one measured for $(MnF_8)^{6-}$ formed in Mn^{2+}-doped CaF_2 [1], whose associated green emission is located at 2.6 eV at ambient pressure. Interestingly, the emission and corresponding excitation spectra for Mn^{2+}-doped CaF_2 and MnF_2 in their high-pressure cotunnite phase are similar, thus indicating that the green S-band emission in MnF_2 is characteristic of ninefold coordinated Mn^{2+}.

In the case of Mn^{2+}-doped CaF_2, where no exciton transfer is permitted, this is the unique RT PL emission. Accordingly, we associate the red D-band emission (1.87 eV) observed in MnF_2 at RT and 16.5 GPa with axially perturbed Mn^{2+} centers, which become populated by energy transfer from regular nearby Mn^{2+} S centers (hereafter named RN): $RN \rightarrow D$. Time-resolved spectros-

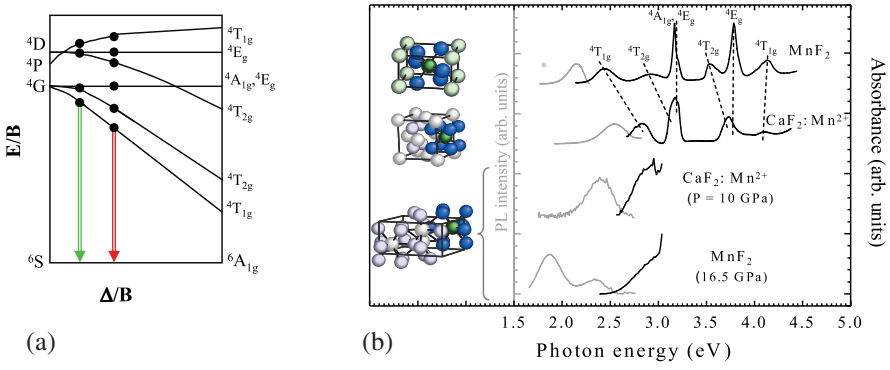

FIG. 2 (color). (a) Tanabe-Sugano diagram for d^5 ions showing the energy level diagram as a function of the O_h crystal-field strength Δ/B, where Δ is the crystal-field splitting energy and B the interelectronic Racah parameter. The diagram explains the different excitation and emission spectra obtained for different Mn^{2+} coordination $(MnF_6)^{4-}$ (red) and $(MnF_8)^{6-}$ (green). (b) Variation of the photoluminescence (in gray) and corresponding excitation spectra of Mn^{2+} in different crystal phases and local structures. The spectra correspond to the optical absorption of MnF_2 at ambient conditions and its emission at $T = 10$ K (asterisk); excitation and emission of CaF_2: Mn^{2+} at ambient conditions; CaF_2: Mn^{2+} at $T = 290$ K and 10 GPa; and MnF_2 at 290 K and 16.5 GPa. The crystal cell and coordination polyhedron at the cation site are shown for each phase. Peak labeling corresponds to the O_h symmetry notation. Note the similarity between the excitation spectra of MnF_2 at 16.5 GPa and CaF_2: Mn^{2+} at 10 GPa in the cotunnite phase $(MnF_9)^{7-}$.

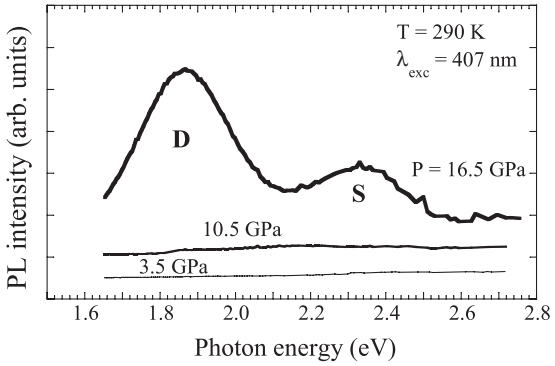

FIG. 3. Variation of the photoluminescence spectra of MnF_2 with pressure at room temperature in the 0–20 GPa range. The MnF_2 was excited into the Mn^{2+} excited states by pumping with a 407 nm laser beam. The two-color photoluminescence bands, D and S, at 1.87 eV (red) and 2.34 eV (green), respectively, correspond to the ${}^4T_1 \rightarrow {}^6A_1$ (O_h symmetry notation) transitions from two different Mn^{2+} centers of MnF_2 in the cotunnite phase.

copy performed in the S and D bands confirms the proposed model (Fig. 4). The intensity time dependence for the red emission indicates that the associated lifetime ($\tau_D^{\text{long}} = 0.9$ ms) is shorter than the green PL lifetime ($\tau_S \sim 5$ ms) despite RN Mn^{2+} transfer to D centers. Although this behavior seems to be contradictory with the long-lived decay time of the green emission, it is consistent with an exciton dynamics involving $RN \rightarrow D$ excitation transfer and largely suppressed exciton migration within regular ninefold coordinated Mn^{2+} ($S \rightarrow S$) in the cotunnite phase. In fact, the D band is the dominant feature of the time-resolved PL spectrum obtained a few

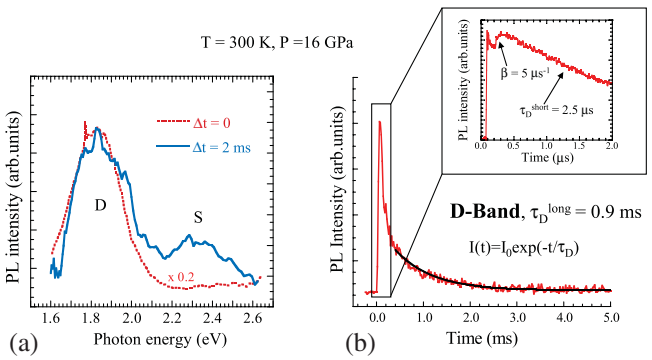

FIG. 4 (color). (a) Time-resolved emission spectra of MnF_2 at 300 K and 16.5 GPa. The emission spectra were obtained by photon-counting techniques measuring for 1 ms immediately after the excitation pulse (red) and 2 ms delayed after the excitation pulse (blue). (b) Time dependence of the PL intensity for the D band at 1.8 eV. The long-decay photoluminescence lifetime is 0.9 ms. The inset shows a magnification of $I(t)$ around 2 μs after the laser pulse. The rise of the photoluminescence intensity for $t > 0.1$ μs reveals transfer phenomena from regular nearby Mn^{2+} sites. The measured transfer rate and the associated short-decay lifetime of the D band are 5 μs^{-1} and 2.5 μs, respectively. The S band shows a decay with an associated lifetime, $\tau_S \approx 5$ ms.

microseconds after the excitation pulse, whereas the S band is enhanced if PL detection is delayed 2 ms [Fig. 4(a)]. The energy transfer involved in the red emission is revealed by the sharp increase ($\sim$0.2 μs) of the time-dependent emission at 1.6 eV before decay [Fig. 4(b)]. Furthermore, the D-Mn^{2+} PL exhibits two different decay processes, which confirm that the energy-transfer $S \rightarrow RN \rightarrow D$ mechanism governs the red PL. In the short-time regime, it decays with $\tau_D^{\text{short}} = 2.5$ μs [Fig. 4(b), inset], basically corresponding to the radiative lifetime of the axially perturbed Mn^{2+} centers (D). This unexpectedly short lifetime for Mn^{2+}, which usually takes values of several milliseconds for oxides and halides [1–3,8,29], is consistent with the increase of the electric-dipole transition probability observed in highly noncentrosymmetric Mn^{2+} in comparison to more centrosymmetric Mn^{2+} centers. In the long-time regime, the D-emission decay ($\tau_D^{\text{long}} = 0.9$ ms) is related to the deexcitation of D-Mn^{2+} centers, which are populated as a result of exciton diffusion from remote S-Mn^{2+} [30,31].

The lifetime for the S band at 16.5 GPa ($\tau_S \approx 5$ ms) decreases as compared with the measured lifetime for isolated $(MnF_9)^{7-}$ centers formed in Mn^{2+}-doped (Sr, Ba)F_2 ($\tau = 13$ ms) at the same pressure in the cotunnite phase [1,2]. This fact reflects additional deexcitation channels for S-Mn^{2+} via $S \rightarrow RN \rightarrow D$ and transfer to nonradiative centers. In our model, the rate equations describing the exciton dynamics for the Mn^{2+} sites are given by

$$\begin{aligned} \frac{dN_D}{dt} &= \beta N_{RN} - \tau_D^{-1} N_D, \\ \frac{dN_{RN}}{dt} &= -(\beta + \tau_S^{-1}) N_{RN} + f(t)\gamma N_S, \\ \frac{dN_S}{dt} &= -\tau_S^{-1} N_S = -[\tau_0^{-1} + \tau_K^{-1} + \gamma] N_S, \end{aligned} \tag{1}$$

where N_D, N_S, and N_{RN} refer to the number of excited axially perturbed (D), regular (S), and regular nearby (RN) Mn^{2+} centers, respectively. The three coupled equations provide the time-dependent intensity for the two emission bands taking values of $\tau_D = \tau_D^{\text{short}} = 2.5$ μs and $\tau_S = 5$ ms for lifetimes, and $\beta = 5$ μs^{-1} and $\gamma = 0.1$ $\text{ms}^{-1} = 0.0001$ μs^{-1} ($\beta \gg \gamma$) for $S \rightarrow S$ and $RN \rightarrow D$ transfer rates, respectively [Fig. 4(b)]. τ_0 is the Mn^{2+} lifetime in absence of migration; $\tau_0 = 13$ ms in CaF_2: Mn^{2+} in the cotunnite phase [1,2]. τ_K^{-1} accounts for transfer to nonradiative centers and $f(t)$ for the time-dependence of the population N_{RN} due to diffusion-limited energy-transfer processes $S \rightarrow RN$ [31]. The model also explains why $\beta \gg \gamma$ through the different exchange coupling between regular S-S Mn^{2+} pairs and D-RN Mn^{2+} pairs. In fact, the energy-transfer rate between two coupled Mn^{2+} centers, named A and B, is given by the Fermi golden rule,

$$\tau_{A\rightarrow B}^{-1} = \frac{2\pi}{\hbar} |\langle A, B^* | H | A^*, B \rangle|^2 \int_E g_A^{\text{exc}}(E) g_B^{\text{emis}}(E) dE. \tag{2}$$

H represents the exchange coupling Hamiltonian responsible for energy transfer between A and B (* stands

for excited state), $g_i(E)$ is the intrinsic transition shape function for $i = A \rightarrow A^*$, $B^* \rightarrow B$ (i.e., the excitation and emission spectral shapes for A and B, respectively) obeying $\int_E g_A^{\mathrm{exc}}(E)dE = \int_E g_B^{\mathrm{emis}}(E)dE = 1$. The overlap integral $\int_E g_A^{\mathrm{exc}}(E) g_B^{\mathrm{emis}}(E)dE$ is the density-of-states factor of the excitation and emission centers, respectively, ensuring energy conservation [32]. This equation justifies not only why $\beta(RN \rightarrow D) \gg \gamma(S \rightarrow S)$, but also why γ strongly decreases on passing from the fluorite and rutile phases to the cotunnite phase in MnF_2 yielding RT PL. Except for the exchange interaction, the main difference between β and γ arises from the big overlap associated with D-ground and RN-excited states, since both RN emission and D excitation, $g_{RN}^{\mathrm{emis}}(E)$ and $g_D^{\mathrm{exc}}(E)$, appear in the same spectral range. For S-S, however, the overlap integral involves $g_S^{\mathrm{emis}}(E)$ and $g_S^{\mathrm{exc}}(E)$ and is therefore strongly reduced due to the large Stokes shift of 0.4 eV between S-emission and S-excitation bands (Fig. 2) [32]. The reduction of $\gamma(S \rightarrow S)$ in the cotunnite phase, which is crucial for the appearance of RT PL in MnF_2, is associated with the decrease of the Mn-F-Mn exchange angle θ on passing from rutile (128°) to fluorite (110°) and cotunnite (90°) phases [9,25,33]. Pressure-induced phase transitions result in a reduction of the exchange interaction and hence the $S \rightarrow S$ transfer rate at high pressure, thus supporting our present findings.

Although the origin of the axially perturbed centers is uncertain, oxygen-bound (or OH-bound) Mn^{2+} [23] is likely responsible for the D-band emission. The presence of one O^{2-} (or OH^-) ligand in $(MnOF_8)^{8-}$ splits the $^4T_1$ excited state due to the axial crystal field, shifting the low-lying Mn^{2+} emitting state to lower energies with respect to the $(MnF_9)^{7-}$ S band. The energy difference of 0.47 eV between D and S agrees with expectations based on the axial crystal field produced by an oxygen ligand at Mn^{2+}, which leads to a splitting of the $^4T_1$ level of about 0.5 eV [24,27].

It is worth noting that rutile and fluorite phases are not PL in MnF_2 at RT. Pressure-induced Mn^{2+} emission appears just above the fluorite-to-cotunnite phase transition at 13 GPa, and thus neither $(MnF_6)^{4-}$ nor $(MnF_8)^{6-}$ seems to be efficient for PL in concentrated materials in contrast to $(MnF_9)^{7-}$. Upon pressure release, the Mn^{2+} PL disappears in the scrutyinite phase. This phase is known to enhance exciton migration and subsequent transfer to nonradiative traps after findings in milled MnF_2 [24].

In conclusion, high-pressure phases of MnF_2 are efficient to reduce exciton migration among Mn^{2+} yielding increased PL efficiency. Accordingly, a two-color PL was induced in MnF_2 at RT in the cotunnite phase above 13 GPa. Although PL is quenched upon pressure release in the scrutyinite phase for $P < 13$ GPa, the present findings highlight the role of high-pressure phases to obtain PL in concentrated materials at RT and provide new insights to improve photoluminescent materials.

Support from the Spanish MEC (No. MAT2005-00099) and the UC (Program I3) is acknowledged.

*Corresponding author.
rodriguf@unican.es

[1] F. Rodriguez *et al.*, J. Chem. Phys. **119**, 8686 (2003).
[2] I. Hernandez and F. Rodriguez, Phys. Rev. B **67**, 012101 (2003).
[3] Y. Suzuki *et al.*, Phys. Rev. B **35**, 4472 (1987).
[4] A. M. Malyarevich *et al.*, J. Opt. Soc. Am. B **19**, 1815 (2002).
[5] M. D. Sturge, Solid State Commun. **9**, 899 (1971).
[6] M. Mortier *et al.*, Phys. Rev. B **67**, 115126 (2003).
[7] Z. M. M. Zhang *et al.*, Appl. Opt. **41**, 1071 (2002).
[8] B. Henderson and G. F. Imbusch, *Optical Spectroscopy of Inorganic Solids* (Oxford University Press, New York, 1989).
[9] R. G. Burns, *Mineralogical Applications of Cristal Field Theory*, Cambridge Topics in Mineral Physics and Chemistry Vol. 5 (Cambridge University Press, Cambridge, 1993), 2nd ed.
[10] P. F. Moulton, J. Opt. Soc. Am. B **3**, 125 (1986).
[11] S. García-Revilla *et al.*, J. Phys. Condens. Matter **14**, 447 (2002).
[12] S. Kiick *et al.*, Phys. Rev. B **57**, 2203 (1998).
[13] Y. Zhydachevskii *et al.*, J. Phys. Condens. Matter **18**, 5389 (2006).
[14] G. Blasse and B. C. Grabmaier, *Luminescent Materials* (Springer, Berlin, 1994).
[15] B. Di Bartolo, *Optical Interactions in Solids* (John Wiley & Sons, London, 1968).
[16] W. W. Holloway *et al.*, Phys. Rev. Lett. **11**, 82 (1963).
[17] M. J. Weber, J. Lumin. **100**, 35 (2002).
[18] F. R. Wunsch and W. Gebhardt, J. Phys. Condens. Matter **1**, 855 (1989).
[19] T. Tsuboi, P. Silfsten, and R. Laiho, Phys. Rev. B **43**, 1135 (1991).
[20] J. M. Flaherty and B. Di Bartolo, Phys. Rev. B **8**, 5232 (1973).
[21] B. Di Bartolo, J. Danko, and D. Pacheco, Phys. Rev. B **35**, 6386 (1987).
[22] R. Greene *et al.*, Phys. Rev. **171**, 600 (1968).
[23] F. Rodriguez *et al.*, J. Phys. (France), Colloq. **46**, C7-155 (1985).
[24] I. Hernandez, Ph.D. thesis, University of Cantabria, 2006.
[25] E. Y. Tonkov, *High Pressure Phase Transformations: A Handbook* (Gordon & Breach, Philadelphia, 1992), and references therein.
[26] J. D. Barnett, S. Block, and G. J. Piermarini, Rev. Sci. Instrum. **44**, 1 (1973).
[27] A. B. P. Lever, *Inorganic Electronic Spectroscopy, Studies in Physical and Theoretical Chemistry* (Elsevier, NewYork, 1984), 2nd ed..
[28] F. Aguado, F. Rodriguez, and P. Nunez, Phys. Rev. B **67**, 205101 (2003).
[29] F. Rodriguez, H. Riesen, and H. U. Gudel, J. Lumin. **50**, 101 (1991).
[30] R. C. Powell and G. Blasse, *Structure and Bonding* (Springer, Heidelberg, 1980), Vol. 42, pp. 43–96.
[31] M. J. Weber, Phys. Rev. B **4**, 2932 (1971).
[32] M. C. M. de Lucas, F. Rodriguez, and M. Moreno, Phys. Status Solidi B **172**, 719 (1992).
[33] A. Martin-Pendas *et al.*, Phys. Rev. B **49**, 5858 (1994).